Proceedings of the
Annual Stability Conference
Structural Stability Research Council
Atlanta, Georgia, April 21-24, 2026

Post-fire behavior of aluminum alloy cross-sections

Kossi Jonas Sama[1], Moufahdilou Ouro-Yendou[2], Yao Sun[3] Liya Li[4]

Abstract
Aluminum alloys are increasingly adopted in structural applications because of their high strength-to-weight ratio and excellent corrosion resistance. However, their mechanical properties degrade markedly at elevated temperatures, and their post-fire performance remains a critical knowledge gap in structural fire design. Although previous studies have experimentally evaluated the residual strength of aluminum alloy cross-sections after fire exposure, the influence of cross-sectional geometry on stability and resistance under these conditions is still not well understood. This research aims to systematically investigate the post-fire behavior of aluminum alloy cross-sections by compiling and analyzing data from recent experimental studies. Particular emphasis will be placed on local buckling behavior and material degradation effects in hollow section geometries. Numerical simulations will be developed to predict the response of aluminum structural elements subjected to elevated temperatures, while parametric studies will be conducted to identify the key parameters governing residual strength. The findings of this research will support the refinement of structural design guidelines and enable safer and more efficient use of aluminum alloys in fire-exposed environments.

1. Introduction

Structural aluminum alloys have become key sustainable materials in civil and structural engineering, increasingly used in bridges, offshore structures, and buildings due to their high strength-to-weight ratio, corrosion resistance, and durability (Sun et al., 2023b, 2024a). However, fire safety remains a major design challenge because aluminum loses stiffness and strength rapidly at relatively low temperatures compared with steel. During fire exposure, structural temperatures can rise quickly, significantly reducing load-carrying capacity. With melting temperatures typically between 600 °C and 660 °C, preventing structural collapse during or after fire is a critical design consideration (Pandey and Young, 2021; Sun et al., 2023a; Wang et al., 2022).

Most research has focused on room-temperature behavior, including material tests, local buckling, and global instability for various section types (Faella et al., 2000; Liu et al., 2015; Mazzolani et al., 2001). Although some studies investigated in-fire behavior, the residual performance of aluminum after fire exposure remains poorly understood. Experimental evidence shows that

[1] Ph.D. student, Université de Sherbrooke, <kossi.jonas.sama@usherbrooke.ca >
[2] Ph.D. student, Université de Sherbrooke, <moufahdilou.ouro-yendou@usherbrooke.ca>
[3] Full Professor, Hunan University, < yaosun@hnu.edu.cn>
[4] Assistant Professor, Université de Sherbrooke, <liya.li@usherbrooke.ca >

elevated temperatures strongly affect post-fire material properties of aluminum alloys. While Young's modulus often remains relatively stable, the 0.2% proof strength and ultimate strength may decrease by more than 80% after exposure to 400-500 °C (Sun et al., 2024a, 2025a). At the same time, aluminum alloys often show increased strain hardening after exposure above about 300 °C, which makes stocky members retain higher residual capacity than predicted by traditional design models. Recent development of high-strength aluminum alloys (HSAA), such as 7075-T6 with yield strengths exceeding 500 MPa, further highlights knowledge gaps, as post-fire data remain limited compared to conventional alloys like 6063-T5. Current standards, including Eurocode 9 (EC9) (European Committee for Standardization, 2007) and the Aluminum Design Manual (ADM) (Aluminum Association, 2020), provide limited guidance on HSAA post-fire behavior, potentially leading to inaccurate stiffness and resistance predictions. Furthermore, investigations into specific cross-sections under post-fire conditions such as channel, square hollow (SHS), and both equal and unequal-leg angle sections reveal a consistent gap between codified design rules and actual structural performance (Sun et al., 2025c). Evaluations of international standards show that they frequently yield excessively conservative and scattered resistance predictions. This conservatism primarily stems from the neglect of the post-fire strain hardening, which significantly enhances the capacity of stocky cross-sections.

To address the current lack of understanding regarding the post-fire performance of aluminum structural elements, particularly the influence of cross-sectional geometry on residual stability and resistance, and the limited validation of existing design provisions, this study examines the post-fire behavior of aluminum structural elements using a purely numerical approach supported by existing experimental data. First, available experimental results from the literature will be collected and systematically compiled to establish a reliable database of post-fire material and structural responses. Second, validated finite element (FE) models will be developed and calibrated against these experimental observations to accurately reproduce the observed behavior. Finally, extensive parametric studies will be conducted on SHS and circular hollow sections (CHS) to evaluate the influence of key geometric and material parameters. The numerical results will then be compared with current design provisions in EC9 and ADM to assess their accuracy and identify potential areas for improvement.

2. Existing Experimental Test

Existing experimental investigations on post-fire aluminium structures can generally be classified into three complementary research scales: material-level testing, cross-section testing, and structural element or system-level studies. At the material level, numerous studies have focused on quantifying the residual mechanical properties of structural aluminium alloys after exposure to elevated temperatures followed by cooling. Experimental programs (Chen et al., 2016; Liu et al., 2019; Summers et al., 2012; Sun et al., 2023b) on alloys such as 5083, 6061-T6, 6082-T6, and 7075-T73 investigated the degradation of yield strength, elastic modulus, ductility, and hardness as functions of peak temperature and cooling regime, establishing temperature-dependent residual stress–strain relationships and identifying irreversible microstructural changes caused by fire exposure.

At the cross-section and member level, research has primarily examined the residual load-bearing capacity and local stability of aluminium members after fire. Stub-column compression tests have been widely adopted to isolate cross-sectional behaviour, including studies on SHS, CHS, channel sections, and H-sections, covering both conventional and high-strength aluminium alloys. These

investigations evaluated post-fire local buckling modes, residual compressive resistance, and the interaction between material degradation and geometric imperfections (Ding et al., 2025; Sun et al., 2023a, 2024b, 2025c; Wang et al., 2025). Recent work has also considered recycled aluminium alloys and advanced numerical validation to support design-oriented resistance models.

At the structural member level, experimental studies have investigated aluminium columns subjected to elevated temperatures, including eccentric compression tests on 6082-T6 aluminium alloy members, which examined strength degradation and instability behaviour under combined thermal and mechanical loading (Ma et al., 2022). Moving to larger structural scales, studies on aluminium bridge structures under fire conditions evaluated global response, load redistribution, and overall system stability, demonstrating the importance of structural continuity and boundary conditions in fire performance (Portnov and Korolchenko, 2023).

3. Numerical Modeling and Validation Results

In the present study, the focus is placed on the post-fire behaviour of aluminium hollow sections under compression at the cross-section level. Numerical models are first developed and validated against available experimental results reported by (Sun et al., 2025c) for SHS and (Ding et al., 2025) for CHS. The measured geometric dimensions, including width Bor diameter D, thickness t, and length L, together with the exposure temperature T, post-fire material properties tested by coupon test, and measured geometric imperfections w_0, are incorporated into the numerical models for validation.

Numerical analyses are carried out using the FE software ABAQUS, where S4R shell elements are adopted, as previously demonstrated to be suitable for fire and post-fire analyses of thin-walled aluminium members (Sun et al., 2025b; Sun and Han, 2025). The measured engineering stress-strain curves obtained from coupon tests are converted into true stress-logarithmic strain relationships prior to implementation in the numerical models to accurately capture large plastic deformations. Boundary conditions and loading arrangements are carefully reproduced to match the experimental setups. Fixed-ended conditions are simulated by coupling end sections to concentric reference points (RPs), with the bottom RP fully restrained and the top RP allowed to translate only in the longitudinal direction. Initial geometric imperfections are introduced through linear buckling analysis (LBA) to obtain the lowest buckling mode, which is subsequently scaled according to measured imperfections and incorporated into geometrically and materially nonlinear analyses with imperfections (GMNIA).

The corresponding validation parameters and results are summarized in **Table 1**, where $N_{\mathrm{u,FE}}$ represents the experimentally measured ultimate resistance and $N_{\mathrm{u,FE}}$ denotes the corresponding numerical predictions. The comparison shows a mean ratio $N_{\mathrm{u,FE}}/ N_{\mathrm{u,Test}}$ of 0.953 with a coefficient of variation (COV) of 0.034, indicating good agreement between the numerical models and the experimental results.

Table 1. Experimental parameters adopted for model validation

		B or D [mm]	t [mm]	L [mm]	T [°C]	$w_{o\,[}$mm]	$N_{u,Test\,[}$mm]	$N_{u,FE}/N_{u,Test}$ [-]
SHS-80 × 5	S1-T25	79.92	5.05	239.0	25	0.14	349.50	0.991
	S1-T100	79.91	4.85	239.7	102	0.14	350.50	0.946
	S1-T200	79.96	5.04	239.7	205	0.16	354.60	1.011
	S1-T250	79.93	4.97	239.1	244	0.15	257.20	0.975
	S1-T350	79.85	4.94	239.3	296	0.11	204.90	0.993
	S1-T400	80.00	4.87	239.7	404	0.16	121.40	0.958
	S1-T500	79.92	4.99	239.8	504	0.14	104.80	1.006
SHS-120 × 5	S2-T25	120.12	4.96	358.2	25	0.22	472.50	0.990
	S2-T100	120.17	4.92	358.3	102	0.19	473.20	0.983
	S2-T200	120.20	4.98	358.2	205	0.24	490.50	0.988
	S2-T250	120.25	4.93	358.0	244	0.26	327.30	0.967
	S2-T300	120.24	5.00	358.6	296	0.22	243.60	0.994
	S2-T400	120.17	4.91	358.3	404	0.22	136.10	0.915
	S2-T500	120.07	4.88	358.2	504	0.22	113.50	0.964
CHS 40 × 1.4	C1-T25	40.00	1.40	120.0	25	0.18	33.85	0.952
	C1-T200	40.00	1.40	120.0	200	0.14	33.64	0.945
	C1-T250	40.00	1.40	120.0	250	0.15	32.47	0.945
	C1-T300	40.00	1.40	120.0	300	0.21	25.06	0.953
	C1-T350	40.00	1.40	120.0	350	0.17	19.42	0.929
	C1-T400	40.00	1.40	120.0	400	0.23	18.06	0.908
	C1-T450	40.00	1.40	120.0	450	0.16	18.54	0.909
	C1-T500	40.00	1.40	120.0	500	0.14	22.75	0.930
CHS 80 × 1.8	C2-T25	80.00	1.80	240.0	25	0.17	80.64	0.946
	C2-T200	80.00	1.80	240.0	200	0.2	79.77	0.966
	C2-T250	80.00	1.80	240.0	250	0.28	77.80	0.948
	C2-T300	80.00	1.80	240.0	300	0.3	62.40	0.929
	C2-T350	80.00	1.80	240.0	350	0.19	49.66	0.913
	C2-T400	80.00	1.80	240.0	400	0.22	41.34	0.903
	C2-T450	80.00	1.80	240.0	450	0.25	44.09	0.912
	C2-T500	80.00	1.80	240.0	500	0.23	54.90	0.906
							Mean	0.953
							COV	0.034

4. Parametric studies

Following validation, extensive parametric studies are conducted to investigate a wider range of parameters, including cross-section geometries, alloy types, temper conditions, and exposure temperatures, with the objective of improving the understanding and prediction of post-fire compressive resistance and local buckling behaviour of aluminium hollow sections. A total of 35 SHS geometries are considered, with widths ranging from 18 to 113 mm and slenderness ratios B/t varying from 8.5 to 75.4. Similarly, 35 CHS geometries are analysed, with diameters ranging from 25 to 160 mm and D/t ratios between 12 and 106.7. Two representative aluminium alloys, 6063-T5 and 7075-T6, are investigated, and their typical post-fire material stress–strain curves are shown in **Fig. 1**. Exposure temperatures of 25°C, 100°C, 200°C, 300°C and 400°C are considered. Consistent with existing experimental observations, the Young's modulus is assumed to remain

nearly unchanged after cooling, whereas the yield strength f_y and ultimate strength f_u decrease with increasing peak temperature. Previous studies have also reported partial strength recovery or slight strengthening when exposure temperatures exceed approximately 500°C, attributed to microstructural transformations during heating and cooling.

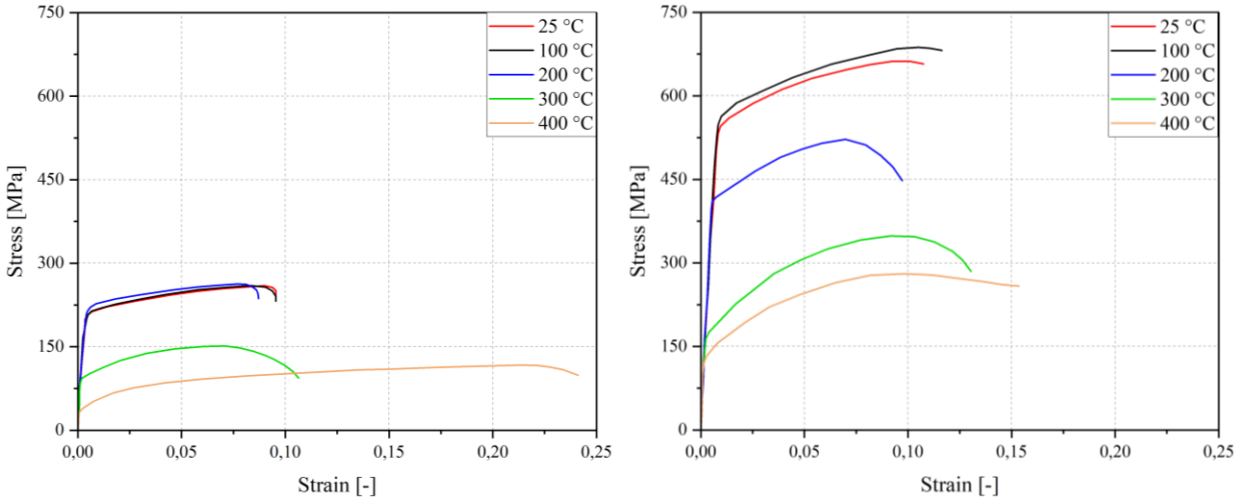

Figure 1: Typical post-fire material stress-strain curves for a) 6063-T5 and b) 7075-T6

The parametric results are presented in **Fig. 2** in the $\lambda_L - \chi_L$ format, expressed in terms of slenderness-based cross-section resistance. The cross-section slenderness λ_L is defined as $\lambda_L = \sqrt{f_{y,T}A/N_{cr}}$, where N_{cr} is the elastic critical load calculated using *HLS* software (Beyer et al., 2021). The reduction factor χ_L is evaluated as $\chi_L = N_{u,\mathrm{FE}}/(f_{y,T}A)$, where $N_{u,\mathrm{FE}}$ represents the ultimate resistance obtained from the FE analysis. The results show a pronounced strain-hardening response, with many cases exhibiting reduction factors χ_L greater than 1.0 and some exceeding 2.0. This behaviour can be attributed to the increase in the $f_{u,T}/f_{y,T}$ ratio with increasing exposure temperature. At higher temperatures, particularly around 400 °C, the aluminium alloys exhibit enhanced ductility and larger elongation capacity, leading to extended post-yield deformation. In addition, SHS sections reach higher cross-section slenderness ranges compared with CHS sections, reflecting the different instability mechanisms governed by plate buckling in SHS and shell buckling in CHS members.

A new design approach based on a slenderness-based formulation is proposed, as summarized in **Table 2** and illustrated in **Fig. 2**. Considering the significant variation in strain-hardening behaviour after fire exposure, separate design curves are proposed to account for the distinct post-fire material responses of different aluminium alloys. Linear design relationships are calibrated to account for the varying strain-hardening behaviour observed. For slender sections, the Ayrton-Perry formulation is adopted to capture the buckling resistance, allowing a consistent representation of instability effects within the proposed design framework. The proposed design method is compared with the existing design provisions of EC9 (European Committee for Standardization, 2007) and CSA S157 ("CSA S157 - Calcul de la résistance mécanique des éléments en aluminium," 2017), as illustrated in **Fig. 3** for CHS and SHS, respectively. The vertical axis represents the ratio between predicted resistance and FE resistance, where values below 1.0 indicate conservative predictions and values above 1.0 indicate unsafe estimations.

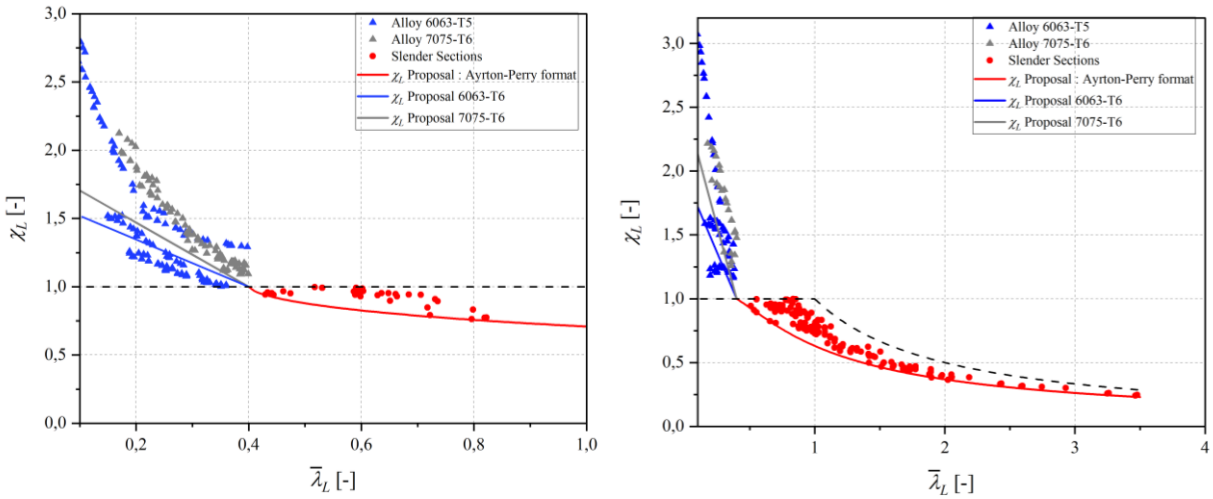

Figure 2: Parametric results for aluminium hollow sections after fire exposure for a) CHS and b) SHS

For CHS shown in **Fig. 3a**, CSA S157 tends to provide conservative predictions for most cases, particularly at low to moderate slenderness levels where post-fire strain hardening leads to enhanced resistance. EC9 also remains generally conservative and does not fully capture the increased resistance associated with the elevated ductility observed after fire exposure. In contrast, the proposed method produces a more uniform distribution of results around unity, demonstrating improved accuracy and reliability over a wide range of slenderness values. For SHS in **Fig. 3b**, a larger scatter is observed due to plate buckling behaviour and the wider attainable slenderness range. Both EC9 and CSA S157 exhibit predominantly unconservative predictions, with many data points exceeding unity, particularly in the high-slenderness region. The proposed design method follows the numerical trends more closely and significantly improves prediction consistency while maintaining safe resistance estimates.

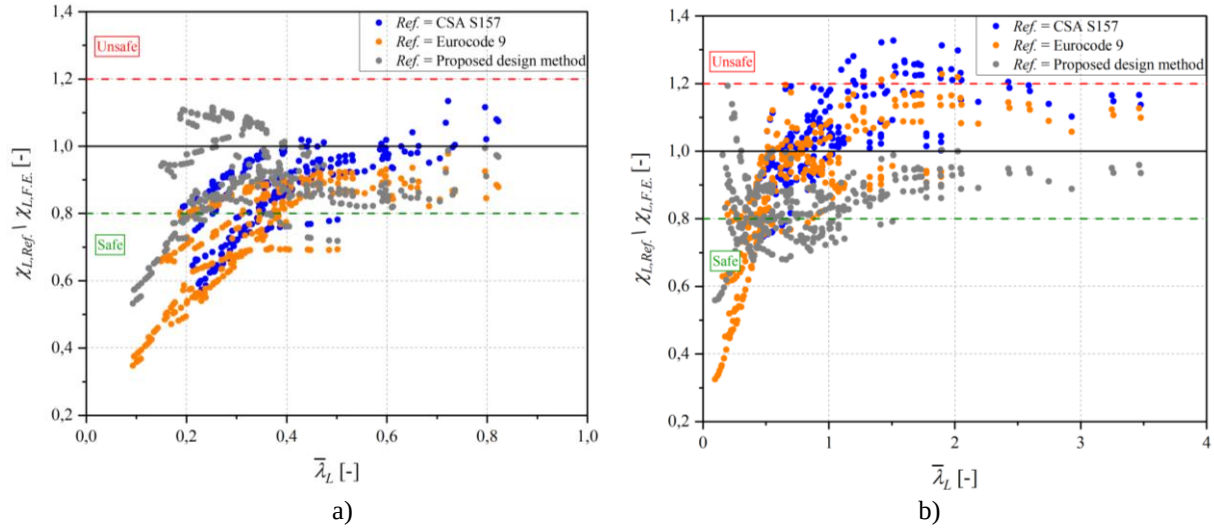

Figure 3: Comparison of design predictions with numerical resistances for post-fire aluminium a) CHS and b) SHS

Table 2. Proposed design equation

CHS		For $\bar{\lambda}_L \leq \lambda_0 = 0.4$:
	Alloy 6063-T5	$\chi_L = -1.8\,\bar{\lambda}_L + 1.7$
	Alloy 7075-T6	$\chi_L = -2.35\,\bar{\lambda}_L + 1.94$
		For $\bar{\lambda}_L > \lambda_0 = 0.4$:
	Ayrton-Perry format	$\Phi_L = 0{,}5 \cdot (1 + \alpha_L \cdot (\bar{\lambda}_L - \lambda_0) + \bar{\lambda}_L^{\,\delta})$
		$\chi_L = \dfrac{1}{\Phi_L + \sqrt{\Phi_L^2 - \bar{\lambda}_L^{\,\delta}}}$
		$\alpha_L = 0.20$ and $\delta = 0.04$
SHS		For $\bar{\lambda}_L \leq \lambda_0 = 0.4$:
	Alloy 6063-T5	$\chi_L = -2.50\,\bar{\lambda}_L + 1.96$
	Alloy 7075-T6	$\chi_L = -3.77\,\bar{\lambda}_L + 2.51$
		For $\bar{\lambda}_L > \lambda_0 = 0.3$:
	Ayrton-Perry format	$\Phi_L = 0{,}5 \cdot (1 + \alpha_L \cdot (\bar{\lambda}_L - \lambda_0) + \bar{\lambda}_L^{\,\delta})$
		$\chi_L = \dfrac{1}{\Phi_L + \sqrt{\Phi_L^2 - \bar{\lambda}_L^{\,\delta}}}$
		$\alpha_L = 0.36$ and $\delta = 0.85$

Table 3 presents the statistical comparison between the proposed design method and the existing design provisions of CSA S157 and EC9 for post-fire aluminium hollow sections, separately evaluated for CHS and SHS members.

For CHS sections, both CSA S157 and EC9 exhibit strong conservatism, with mean resistance ratios of 0.78 and 0.74, respectively, and a large proportion of predictions falling below 0.9. The proposed design method significantly reduces this conservatism, achieving a mean value closer to unity (0.90) while maintaining a low coefficient of variation (COV = 0.14). Although a higher proportion of predictions exceeds unity compared with existing provisions, the overall distribution remains balanced and consistent.

For SHS sections, CSA S157 and EC9 show higher mean values but also larger scatter and a notable proportion of unconservative predictions, particularly for higher resistance ratios. In contrast, the proposed design method yields the lowest COV (0.12), indicating improved prediction consistency. The results demonstrate that the proposed approach provides a more uniform and reliable estimation of post-fire resistance across different cross-section types.

Table 3. Statistical evaluation of different design methods for post-fire aluminium hollow section

Section	Statistic	CSA S157	EC9	Proposed design method
CHS	Mean ($\chi_{L,Ref}/\chi_{L,FE}$)	0.78	0.74	0.90
	COV	0.22	0.20	0.14
	Proportion > 1.0 (%)	4.00	0.00	21.43
	Proportion > 1.1 (%)	0.57	0.00	3.43
	Proportion > 1.2 (%)	0.00	0.00	0.00
	Proportion < 0.9 (%)	68.57	91.14	54.29
	Proportion < 0.8 (%)	44.86	54.57	18.00
SHS	Mean ($\chi_{L,Ref}/\chi_{L,FE}$)	0.91	0.88	0.83
	COV	0.25	0.22	0.12
	Proportion > 1.0 (%)	40.57	27.71	3.43
	Proportion > 1.1 (%)	19.71	11.14	1.14
	Proportion > 1.2 (%)	8.57	1.14	0.29
	Proportion < 0.9 (%)	41.71	45.14	79.43
	Proportion < 0.8 (%)	28.29	29.14	38.29

5. Conclusion and Future work

This study investigated the post-fire behaviour of aluminium hollow sections through validated numerical modelling and extensive parametric analyses. The main conclusions are:

1. Numerical models developed in ABAQUS successfully reproduced the experimental behaviour of post-fire aluminium SHS and CHS sections, showing good agreement in terms of ultimate resistance.
2. Parametric analyses demonstrated that post-fire aluminium hollow sections exhibit pronounced strain-hardening behaviour. The increase in the f_u/f_y ratio after fire exposure, particularly at elevated temperatures, leads to enhanced ductility and higher apparent cross-section resistance.
3. Existing design provisions in EC9 and CSA S157 do not adequately capture post-fire behaviour. Both generally provide conservative predictions, while become unconservative for certain slender SHS sections, especially at higher slenderness levels.
4. A new slenderness-based design approach was proposed to account for different post-fire material responses of aluminium alloys. The proposed method provides improved accuracy, reduced scatter, and balanced safety across a wide range of cross-section slenderness.

Future research will focus on extending the proposed design framework beyond CHS and SHS cross-section resistance. Experimental and numerical investigations on other cross-section shapes and member-level behaviour are needed to support future development of unified post-fire design provisions for aluminium structures.

References

Aluminum Association, 2020. Aluminum Design Manual: 2020. Aluminum Association, Washington, D.C.

Beyer, A., Gardner, L., Meng, X., Taras, A., 2021. Reliability assessment for the Generalized Slenderness based Resistance Method for circular and elliptical hollow sections. ce/papers 4, 2140–2148. https://doi.org/10.1002/cepa.1532

Chen, Z., Lu, J., Liu, H., Liao, X., 2016. Experimental investigation on the post-fire mechanical properties of structural aluminum alloys 6061-T6 and 7075-T73. Thin-Walled Struct. 106, 187–200.

CSA S157 - Calcul de la résistance mécanique des éléments en aluminium, 2017.

Ding, Z., Zhang, W., Xue, X., Sun, R., Hua, J., 2025. Compressive resistance of aluminium alloy circular hollow section stub column after fire exposure. J. Build. Eng. 111, 113253.

European Committee for Standardization, 2007. Eurocode 9: Design of aluminium structures - Part 1-1: General structural rules. Commission of the European Community, Brussels, Belgium.

Faella, C., Mazzolani, F.M., Piluso, V., Rizzano, G., 2000. Local Buckling of Aluminum Members: Testing and Classification. J. Struct. Eng. 126, 353–360. https://doi.org/10/cbc8dx

Liu, M., Zhang, L., Wang, P., Chang, Y., 2015. Experimental investigation on local buckling behaviors of stiffened closed-section thin-walled aluminum alloy columns under compression. Thin-Walled Struct. 94, 188–198. https://doi.org/10.1016/j.tws.2015.04.012

Liu, Y., Liu, H., Chen, Z., 2019. Post-fire mechanical properties of aluminum alloy 6082-T6. Constr. Build. Mater. 196, 256–266.

Ma, H., Hou, Q., Jiang, Y., Yu, Z., 2022. Mechanical performance of 6082-T6 aluminum alloy columns under eccentric compression at elevated temperatures. Thin-Walled Struct. 171, 108824.

Manual of geometric properties of extruded aluminium sections, n.d.

Mazzolani, F.M., Piluso, V., Rizzano, G., 2001. Experimental analysis of aluminum alloy channels subjected to local buckling under uniform compression, in: Proc., CTA, Italian Conf. on Steel Construction, ACS, Milano, Italy. pp. 1–10.

Pandey, M., Young, B., 2021. Post-fire behaviour of cold-formed high strength steel tubular T- and X-joints. J. Constr. Steel Res. 186, 106859. https://doi.org/10.1016/j.jcsr.2021.106859

Portnov, F.A., Korolchenko, D.A., 2023. Aluminium Bridges under Fire Conditions: Structural Behaviour. Buildings 13. https://doi.org/10.3390/buildings13071669

Summers, P.T., Matulich, R.D., Case, S.W., Lattimer, B., 2012. Post-fire mechanical properties and hardness of 5083 and 6082 aluminum alloys, in: ASME International Mechanical Engineering Congress and Exposition. American Society of Mechanical Engineers, pp. 1251–1259.

Sun, Y., Cheng, W., Chen, K., 2024a. Experimental study of in-fire and post-fire material response of high-strength aluminium alloys. J. Build. Eng. 91, 109581. https://doi.org/10.1016/j.jobe.2024.109581

Sun, Y., Cheng, W., Chen, K., Di Sarno, L., 2025a. Experimental and numerical study of high-strength aluminum alloy circular hollow sections after exposure to fire. J. Build. Eng. 111, 113185. https://doi.org/10.1016/j.jobe.2025.113185

Sun, Y., Cheng, W., Chen, K., Di Sarno, L., 2025b. Experimental and numerical study of high-strength aluminum alloy circular hollow sections after exposure to fire. J. Build. Eng. 111, 113185.
Sun, Y., Fu, Z., Song, Y., Xia, J., 2023a. Cross-Sectional Behavior of Aluminum Alloy Channel Section Stub Columns after Exposure to Fire. J. Struct. Eng. 149, 04023085. https://doi.org/10.1061/JSENDH.STENG-12383
Sun, Y., Han, G., 2025. Post-fire capacity of aluminium alloy rectangular hollow sections under compression. Eng. Struct. 327, 119602. https://doi.org/10.1016/j.engstruct.2024.119602
Sun, Y., Li, M., Chen, X., Raffoul, S., 2025c. Material response and local behaviour of post-fire aluminium alloy square hollow sections. J. Constr. Steel Res. 227, 109392. https://doi.org/10.1016/j.jcsr.2025.109392
Sun, Y., Wang, Z., Xia, J., Sarquis, F.R., De Lima, L.R.O., 2024b. Experimental and numerical study of aluminium alloy angle-section stub columns. Thin-Walled Struct. 205, 112361. https://doi.org/10.1016/j.tws.2024.112361
Sun, Y., Zhang, K., Gong, G., 2023b. Material properties of structural aluminium alloys after exposure to fire. Structures 55, 2105–2111. https://doi.org/10.1016/j.istruc.2023.07.027
Wang, Z., Li, J., Ouyang, Y., Zhao, O., 2025. Post-fire local buckling of recycled 6061-T6 aluminium alloy SHS stub columns. Eng. Struct. 343, 120972.
Wang, Z., Li, M., Han, Q., Yun, X., Zhou, K., Gardner, L., Mazzolani, F.M., 2022. Structural fire behaviour of aluminium alloy structures: Review and outlook. Eng. Struct. 268. https://doi.org/10.1016/j.engstruct.2022.114746